Article:
Wu, B.-N., Li, J.-X., Ding, H.-H. et al. (2024) Study on the optimization of solid particle additives in top-of-rail friction modifiers based on a twin-disc testing apparatus. International Journal of Rail Transportation, 13 (5). pp. 928-948. ISSN: 2324-8378

https://doi.org/10.1080/23248378.2024.2438701

Study on the optimization of solid particle additives in top-of-rail friction modifiers based on a twin-disc testing apparatus

Bing-nan Wu[a], Jia-xin Li[a], Hao-hao Ding[a, e], Lu-bing Shi[a,b], Xin-xin Song[a], Jun Guo[a], Shu-yue Zhang[a, e, *], Wen-jian Wang[a, e, *] , Roger Lewis[c] and Enrico Meli[d]

a. Tribology Research Institute, State Key Laboratory of Rail Transit Vehicle System, Southwest Jiaotong University, Chengdu 610031, China

b. Zhengzhou Research Institute of Mechanical Engineering Co., Ltd., Zhengzhou 450001, China

c. Department of Mechanical Engineering, The University of Sheffield, Mappin Street, Sheffield S1 3JD, UK

d. Department of Industrial Engineering, University of Florence, Florence 50139, Tuscany, Italy

e. Mechanical Industry Key Laboratory of Damage Mechanism and Protection Technology for High-speed Friction Pairs, Southwest Jiaotong University, Chengdu 610031, China

∗Corresponding author. Tel: +86-28-87634304.

E-mail address: zhangsy@swjtu.edu.cn (Shu-yue Zhang)

wwj527@swjtu.cn (Wen-jian Wang)

Study on the optimization of solid particle additives in top-of-rail friction modifiers based on a twin-disc testing apparatus

Abstract: Top-of-rail friction modifiers are used to manage the friction on the top-of-rail and help alleviate corrugation, reduce noise, decrease material wear, etc. In this paper, five series of FM samples were prepared and tested using a twin-disc testing apparatus to optimize the solid particles in the FM, aiming to achieve an intermediate adhesion level and a positive creep curve at the wheel-rail interface. The roles of every composition were explored and further the mass content of solid particles, the mass content ratio of lubrication to modifying particles, and the hardness and size of modifying particles were optimized. The possible influence mechanism of FM third body layer shear strength on the wheel-rail adhesion behavior was discussed based on the Coulomb-Mohr theory. The FM sample containing 76.31 wt% of water, 2.77 wt% of carboxymethyl cellulose (CMC), 10.46 wt% of resin, 3.04 wt% of graphite particles, and 9.13 wt% of kaolin particles can reduce adhesion coefficient to 0.129 and generate an obvious positive creep curve in the wheel-rail interface.

Keywords: Wheel-rail adhesion; Friction modifier; Solid particles; Modifying particles

1. Introduction

The rapid development of railways has caused serious damage to an important component, the wheel and rail interface [1, 2]. In recent years, top-of-rail (TOR) products have been used globally to manage the friction between the wheel tread and the top-of-rail, thereby protecting wheel-rail materials [3, 4]. As a cost-effective wheel-rail interface maintenance technique, the application of top-of-rail products can improve the efficiency, quality, safety, and economy of railway transportation. For example, Transport Canada found that the application of friction modifiers on a heavy-haul rail line could decrease about 9.6% of the average energy

consumption of locomotives [5], reducing the operating costs of the heavy-haul rail line.

A top-of-rail product can produce a moderate friction level under a range of material application rates [6]. This moderate friction level not only ensures sufficient traction and braking performance of the train but also brings many benefits, such as reducing wheel-rail wear and rolling contact fatigue (RCF) [7, 8], lowering friction noise and squealing [9], decreasing train derailment coefficient [10], and reducing energy consumption in operation [11]. In addition, it can alleviate wheel-rail corrugation by producing a positive friction, where the adhesion coefficient increases with the creepage [12], to eliminate roll-slip oscillation [13]. The appropriate application of top-of-rail products includes a proper application amount [14] and a well wheel-rail contact interface, in which there are not a large number of RCF cracks as this would pose a risk of exacerbating RCF development in top-of-rail products. [7, 14].

Friction modifiers (FMs) are water-based TOR products with characteristics such as dryness, eco-friendliness, and ease of cleaning. However, compared with oil or grease-based TOR products, FMs have several disadvantages, such as lower retentivity, shorter carry distance [6], and higher application amount. These limitations are due to the drying behavior of FMs. After the water in FMs evaporates, an FM third body layer, formed from the residual substances of FMs and wheel-rail material debris, cannot be transferred further along the track by passing wheels [15]. This could decrease the friction control performance of FM on the entire target curve. Therefore, appropriate additives are required to improve the tribological properties of FMs.

Solid particles, which can be divided into lubrication particles and modifying particles, are important additives in all types of TOR products [14, 16-18]. Lubrication particles, such as

molybdenum disulfide and graphite particles, act to reduce friction while modifying particles are used to inhibit excessive lubrication. Modifying particles are usually minerals such as barite, zinc oxide, aluminum oxide, and talc [16, 18]. Galas et al. [16] pointed out that the remaining mineral particles could provide a stable and suitable adhesion level, and zinc oxide particles seemed to be a suitable modifying particle because they ensure faster recovery speed of adhesion coefficient. Zakharova et al. [18] established that barite particles could be the best filler in carboxymethyl cellulose to give the most stable friction characteristics. The influence mechanism of solid particles on the friction control performance of FMs can be explained by shear strength theory [6, 19, 20]. Solid particles along with their suspension system constitute a unified entity that jointly bears the wheel-rail forces whether in wet or dry conditions. Compared with metal asperities, the FM third body layer with lower shear strength can provide a shear displacement compensation for the wheel-rail interface, thereby producing a desired friction level. However, it is difficult to accurately and directly quantify the shear displacement compensation effect of FMs in the wheel-rail contact interface, and there are limited studies on the optimization of the particles or mixtures of particles to achieve an appropriate adhesion coefficient over a range of condition.

In this paper, five series of FM samples were prepared and tested using a twin-disc testing apparatus to optimize the solid particles in the FM, aiming to achieve an intermediate adhesion level and a positive creep curve at the wheel-rail interface. The roles of each composition in the FM material system and two key adhesion parameters were acquired in the test of the first series of FM samples. For the following series of FM samples, the mass content of solid particles, the mass content ratio of lubrication particles to modifying particles, and the hardness and size of

modifying particles were optimized. Finally, an FM sample with good retentivity and no risk of low adhesion after application was obtained.

2. Experimental methodology and details

2.1 Design and preparation of FM

For the FM preparation process, deionized water, carboxymethyl cellulose (CMC, CAS 9004-32-4), acrylic resin emulsion (resin), graphite particles (lubrication particles), and five types of modifying particles were chosen as the material compositions. SEM images of all constituents (except deionized water) used in this study are shown in Figure 1.

The purpose of using deionized water was to avoid the influence of anions or cations on colloidal particles composed of a CMC network structure and solid particles [21]. Pure deionized water cannot hold the heavy solid particles to form a stable suspension system, so CMC and acrylic resin were chosen as two other additional additives to improve the suspension and film-forming properties of the FM material system.

CMC is a solid powder with good water solubility, biodegradability, and thermal stability. An aqueous solution with appropriate CMC concentration is a high-viscosity gel, and densely packed and entangled molecular chains can hold solid particles in place to avoid sedimentation [21, 22]. A previous study showed that a 3.6% mass fraction solution of CMC exhibits good rheological performance in the FM material system [23]. On the other hand, the resin was chosen as an additional liquid carrier composition due to its lower glass transition temperature (about 16℃) and excellent wear resistance, which contributes to improving the film-forming performance of the FM material system. Graphite particles are widely used in the design of water-based lubricants due to their good lubricity and stability [24]. Accordingly, graphite

particles were chosen as lubrication particles, and the other particles were chosen as modifying particles. The test reports provided by the material suppliers show that the purity of all additives is above 98%.

Detailed information about the five series of FM samples is shown in Table 1. The lubrication particles in these FM samples were graphite particles with a particle size of 0.1 μm. The purposes of preparing and testing these five series of FM samples, as well as the modifying particles used in each series, are as follows:

(1) For series A, FM samples were used to explore the roles of each additive in the FM material system and identify key parameters affecting wheel-rail adhesion. The modifying particles in series A were talc particles.

(2) For series B, FM samples were used to explore the influence of the mass content of solid particles on wheel-rail adhesion. The total mass content of lubrication and modifying particles increased from 9.25% to 17.24%. The modifying particles in Series B were talc particles.

(3) In series C, FM samples were designed to explore the effect of the mass content ratio of lubrication particles to modifying particles on wheel-rail adhesion. The mass content of modifying particles was increased from 5.23% to 8.72%, while the mass content of lubrication particles was decreased from 5.23% to 1.74%. The modifying particles in series C were talc particles.

(4) In series D, FM samples were used to investigate the effect of the hardness of modifying particles on wheel-rail adhesion. Talc particles (Mohs hardness 1-2) were replaced with particles of higher hardness, such as zinc oxide particles (4), kaolin particles (4-5), silicon

dioxide particles (6-7), and aluminum oxide particles (8.8).

(5) In series E, FM samples were used to study the influence of modifying particle size on wheel-rail adhesion. The particle size of kaolin particles was increased from 0.8 μm to 12 μm. The particle size of modifying particles was about 8 μm in series A to D.

The FM preparation process was as follows (Figure 2): (1) The first step was to put CMC into deionized water and then stir the solution into a transparent colloid. (2) The second step was to add the graphite particles and the modifying particles and then stir the mixture until there was no precipitation. (3) The next step was to add the resin to the above solution and continue stirring until there was no change in the solution. (4) The final step was to let the solution stand at room temperature for one week to fully extend the CMC molecular grid structure. The speed of the mixer was 500 RPM during the preparation process. The appearance of series A FM samples is shown in Figure 3. Series B to E of FM samples exhibited the same appearance as the A7 sample.

2.2 Testing apparatus and wheel-rail samples

A twin-disc testing apparatus (MJP-30A, Figure 4) was used to simulate the real wheel-rail contact condition. The twin-disc testing machine has two rollers with a diameter of 60 mm, driven by two 7.5 kW servo motors. The creepage (λ) can be adjusted by setting different rotational speeds of the rollers (ω) according to Equation 1. The vertical force (F_v) between the two rollers is applied by a hydraulic cylinder placed at the end of the lever arm and measured by a pressure sensor at the bottom of the hydraulic cylinder. The tangential force (F_t), which is the longitudinal frictional force between two rollers (Figure. 4c), is calculated using the friction torque (M) and the radius of the rollers (r). The friction torque(M) is collected by a torque sensor

mounted on the shaft that supports the wheel roller. The adhesion coefficient (μ) between the two rollers can be calculated in real-time according to Equation 2. The number of cycles in this paper refers to the number of cycles of the lower specimen (wheel sample) on the twin-disc testing apparatus.

$$Creepage = \frac{\omega_{rail} r_{rail} - \omega_{wheel} r_{wheel}}{\omega_{rail} r_{rail}} = \frac{\omega_{rail} - \omega_{wheel}}{\omega_{rail}} \quad (1)$$

$$\mu = \frac{M}{F_v r} \quad (2)$$

The wheel and rail rollers were sampled from C-class wheel tread and U75V railhead, respectively. The chemical compositions and hardness of wheel and rail rollers are listed in Table 2. The initial surface roughness of rollers was about 0.1 μm. Before applying FM to the contact interface of the two rollers, there was a running-in phase for the roller contact surfaces to reach a stable worn condition. This phase was carried out under dry conditions for 5000 cycles (1100 MPa, 1% creepage). After the running-in phase, the surface roughness of the worn wheel and rail rollers was about 0.6 μm and 0.3 μm, respectively.

Besides, viscosity is an important indicator of the internal friction level in the FM material system. Therefore, a rotational viscometer (NDJ-8s, Figure 5a) was used to test the rotational viscosities of each FM sample using a #4 rotator at a rotational speed of 0.3 RPM (revolutions per minute).

2.3 Experimental methods and parameters

On the twin-disc testing apparatus, the vertical force between the wheel and rail rollers was set to 2520N. This vertical force generates a Hertzian contact pressure of approximately 1100 MPa, equivalent to the axle load of a 21-ton locomotive. Therefore, it is feasible to study the effect of FM on wheel-rail adhesion at this normal force level. The rotational speed of the wheel

roller was maintained at 500 RPM.

Two types of wheel-rail adhesion tests were carried out. Figure 6a shows a schematic of the expected adhesion curve for the first type of test, the lowest adhesion coefficient and retentivity were obtained in this test. The FM application amount is an important test parameter. Xavier et al. [25] proposed a method to convert the field FM application amount (from a wayside applicator) into an appropriate amount for the scaled-down twin-disc contact, which was about 0.0209 g, based on the diameters of rollers and wheels. Although the diameter of rollers in this study was smaller than those Xavier et al. used, the parameters of creepage and rotational speed were higher than those used by Xavier et al. Therefore, 20 μL was chosen as the application amount in the first test. The test step was as follows: the FM sample to be tested was added into the contact interface of rollers by a manual dispenser (Eppendorf, Multipette M4, accuracy of 1 μL) in the application amount of 20 μL, as shown in Figure 5c. In the FM application process, the FM was applied to the simulated wheel-rail interface by the manual dispenser in one second, because the transition of the actual wheel-rail interface from a dry state into FM state is very short. Besides, the variation in the application amount of FM with each use of the manual dispenser was less than 1 μL, ensuring good repeatability. The lowest adhesion coefficient after applying FM samples was recorded, and then the number of wheel roller cycles experienced from the lowest adhesion to 0.3 was recorded as the retentivity.

In the second type of test, the influence of FM on the creep curve was evaluated through three stages (Figure 6b) which was used by Gutsulyak et al. [26]. In the first stage, the rollers were run at a low creepage (0.3%) to obtain a running-in contact interface. Then a 60 μL FM sample was applied to the wheel-rail interface. Compared with the first type of test, the purpose

of increasing the FM application amount was to compensate for the FM loss during the film-forming stage (second stage), ensuring that the surface of the rollers had a sufficient FM third-body layer at the initial moment of the testing stage (third stage). In the second stage, the FM underwent a running-in process, in which the FM sample was crushed and dried. After that, a dried FM third-body film was formed on the disc surfaces. In the third stage, creepage was adjusted from 0.3% to a required test level, which was 0.3 %, 0.6 %, 1 %, 2 %, or 5 %. The average adhesion coefficient in the third testing stage was recorded as the adhesion coefficient at the testing creepage (across the 500 cycles stage duration). Then the creep curve was plotted to judge the type of creep curve according to Figure 6c. For FMs, the target is a positive friction curve.

3 Results

3.1 Base compositions and wheel-rail adhesion parameters

Figure 7 and 8 respectively show the results from the first and the second type of tests for series A of FM samples. After applying deionized water (A1, Figure 7a), the adhesion coefficient initially decreased to 0.25 and then decreased to 0.23 after about 20 cycles. This is because the viscosity of the third-body layer formed by the mixture of water and oxide/wear debris is greater than that of water, leading to a secondary decrease in the adhesion coefficient under mixed lubrication conditions [27, 28]. Subsequently, the adhesion coefficient increased almost vertically back to the dry state. This occurred as the third body layer was sheared off all at once rather than depleting slowly. The creep curve of the deionized water exhibits a very pronounced positive friction (Figure 8). Compared to deionized water, the high-viscosity CMC solution (A3) caused a more significant decrease in the adhesion coefficient, approximately

0.18 (Figure 7b). Meanwhile, the slope and level of positive friction were lower than that of only applying deionized water (Figure 8).

After applying resin (Figure 7c), the adhesion coefficient initially decreased to 0.086 then quickly increased to 0.128, after which the adhesion coefficient gradually recovered to the dry state at almost a linear rate of approximately $0.5\text{^}10^{-4}$/cycle. The application of resin produced a slightly negative creep curve (Figure 8) with a lower adhesion level than that of the CMC solution or water alone. A significant amount of resin was squeezed out of the wheel-rail contact zone, and the remaining dried quickly in the contact zone (resin has a lower drying temperature), which explains the sharp decrease in adhesion coefficient. The long and slow recovery process of the adhesion coefficient back towards a dry value resulted from the good wear resistance of the resin layer. Compared to pure resin, the application of diluted resin (A4, Figure 7d) resulted in a lower adhesion coefficient, faster recovery speed, and a neutral creep curve. This could be attributed to the water enhancing the fluidity of the resin, which means that it spread across the roller surfaces and squeezed out of the contact more easily.

After applying the A5 samples containing deionized water, resin, and CMC, the adhesion coefficient decreased to 0.096 and then recovered to 0.23 at a fast speed (Figure 7e), producing a positive friction at a moderate adhesion level (Figure 8). The addition of a 10.46 % mass fraction of talc particles (A6, Figure 7f) and graphite particles (A7, Figure 7g), respectively, caused obvious changes in the adhesion coefficient and creep curve. Talc particles, as the modifying particles, increased the level of the lowest adhesion coefficient and the slope of the positive friction while shortening the retentivity. In contrast, graphite particles had the opposite effect compared to talc particles. Although these two particles cannot be used alone as solid

particles in FM samples, the friction control performance of FMs could be optimized by appropriately setting the parameters of these two kinds of particles.

The above test results show that the adhesion recovery process after applying FM samples has many characteristics. For example, a higher adhesion coefficient is accompanied by a lower retentivity and a faster adhesion coefficient recovery speed. Therefore, seven parameters are used to describe the adhesion recovery process, including the lowest adhesion coefficient, retentivity, number of cycles in the rapid recovery stage, the slope in the rapid recovery stage, adhesion coefficient at 0.6 % creepage, the slope in the slow recovery stage, and York linear regression slope of the creep curve after 0.6% creepage. These parameters are named datasets (a) to (g) in order. The relationship between different parameters is shown in Figure 9.

Figure 9a shows that as the retentivity of FM samples increased, the lowest adhesion coefficient decreased, except for A3. This suggests that the FM sample composed of constituents used in series A cannot simultaneously control the adhesion coefficient of the wheel-rail interface at a moderate level while exhibiting strong retentivity. The resin possesses the characteristics of rapid drying and excellent wear resistance, resulting in A3 becoming a singular point.

Speed parameters in the adhesion recovery process can reflect the drying speed and shear strength of the FM samples. According to the results in Figure 9b, the retentivity consists of an initial rapid recovery stage followed by a slow recovery stage. Due to the unique lubrication mechanisms of the FM samples, the creep curves obtained using the second type of test are discrete data points. Thus, it is inaccurate to use the common creep model, such as the FASTSIM or POLACH numerical calculation model, to fit a continuous creep curve. The York

linear regression analysis method considers the errors in variables during the calculation process, making it suitable for linear regression analysis of high-dispersity data sets, particularly for estimating linear creep curves. Therefore, this study employed York linear regression analysis to estimate the slope of the curve after 0.6% creepage. The York linear regression analysis typically includes processes such as calculating initial estimates, computing errors, applying weighted least squares, and iterative optimization. The calculation method of York linear regression analysis can be seen in [29]. This slope and the adhesion coefficient at 0.6% were chosen as parameters to analyze the friction characteristics.

To streamline the adhesion coefficient parameters, the Pearson Correlation Coefficient [30] was employed to find representative parameters. The Pearson Correlation Coefficient is a statistic that measures the degree of linear correlation between two variables, with a range from -1 to 1. When the Pearson correlation coefficient is -1, 0, or 1, it represents the following relationships between two variables: -1 indicates a perfect negative correlation, 0 indicates no correlation, and 1 indicates a perfect positive correlation. However, the Pearson correlation coefficient can only detect linear relationships and may not effectively capture non-linear relationships. The calculation method of the Pearson correlation coefficient can be seen in [30]. The Pearson Correlation between each dataset are shown in Figure 9d. It can be observed that there is a very strong correlation between the six parameters except for the York linear regression slope, especially the lowest adhesion coefficient (a), which exhibits a very strong correlation with the other five parameters. Therefore, the lowest adhesion coefficient and the York linear regression slope were considered as evaluation parameters in the subsequent optimization experiments of the solid particle parameters.

3.2 The mass content and ratio of lubrication particles to modifying particles

The series B of FM samples was made by increasing the mass content of solid particles (graphite particles and talc particles) from 9.25% to 17.24% in a mixing solution of CMC aqueous and resin, decreasing the mass content of deionized water, and keeping the mass content ratio of graphite particles to talc particles at 1:1. Figure 10 shows the rotational viscosities of series B of FM samples and their influence on wheel-rail adhesion. As the mass content of solid particles increased, the rotational viscosity of the FM sample increased from 199.8 Pa·s to 242 Pa·s, the lowest adhesion coefficient decreased from 0.103 to 0.085, and the slope of positive friction remained almost unchanged.

According to the simulation calculation results of Li et al. [31, 32], the application of FM samples can produce a mixed lubrication condition at the simulated wheel-rail contact interface. The rise in FM viscosity will increase the film thickness formed in the contact and increase the degree of surface separation, causing a reduction in friction. Lower adhesion coefficients were produced by applying FM samples with higher viscosity, such as B4 or B5 (Figure 10b and d). An increase in the number of lubrication particles may reduce the shear strength of the FM third body layer. Therefore, the recovery rate of the adhesion coefficient was reduced by FM samples with higher mass content of solid particles (Figure 10b). The test results of series B indicate that adjusting the solid particle content does not efficiently regulate the lowest adhesion coefficient level (0.085~0.103) or alter the slope of the creep curve. The solid particle content in the FM that leads to a 'safe' adhesion coefficient of 0.1 is about 10 % (B2).

Based on the FM sample B2, the series C FM samples were made by increasing the mass content ratio of talc particles to graphite particles from 1:1 to 5:1 while keeping the mass content

of deionized water and solid particles at 76.31 % and 10.46 %, respectively. The increase in the mass content ratio of modifying particles to lubrication particles had little influence on the rotational viscosity (Figure 11a) and increased the lowest adhesion coefficient from 0.094 to 0.128 (Figure 11b). In adhesion, the slope of the creep curve increased significantly (Figure 11c).

The mass content ratio of modifying particles to lubrication particles might exert its influence on the wheel-rail adhesion by changing the shear strength of the FM third-body material. Compared with lamellar graphite particles (Figure 1), irregular talc particles can enhance the internal friction within the material, thereby improving its shear strength. Accordingly, the lowest adhesion coefficient and the rate of the adhesion recovery process both increased. The mass content ratio of modifying particles to lubrication particles in the FM corresponding to a 'safe' adhesion coefficient of 0.1 is 3:1 (C3).

3.3 The hardness and particle size of modifying particles

Based on the C3 sample, the talc particles (Mohs hardness 1~2) were replaced with harder modifying particles, such as zinc oxide particles (Mohs hardness 4), kaolin particles (Mohs hardness 4-5), silicon dioxide particles (Mohs hardness 6-7), and aluminum oxide particles (Mohs hardness 8.8) in the series D of FM samples. The mass content of lubrication particles and modifying particles were 3.04 % and 9.12 %, respectively. When the Mohs hardness of the modifying particles in the FM increased from 1 to 8.8, the rotational viscosity was about 229 Pa·s (Figure 12a), the lowest adhesion coefficient increased from 0.101 to 0.144 (Figure 12b), and the slope of the creep curve increased from $0.01\%^{-1}$ to $0.033\%^{-1}$ (Figure 12c).

The influencing mechanism of modifying particle hardness on the wheel-rail adhesion

coefficient was consistent with that of increasing the mass fraction of modifying particles, but its influence was more pronounced. Among the five kinds of modifying particles, kaolin particles with moderate hardness can adjust the adhesion coefficient to a moderate level and enable the FM to have prolonged retentivity.

Based on the D3 sample, the particle size range of kaolin particles was expanded from 8 μm to a range from 0.8 μm to 12 μm in the series E FMs. The rotational viscosities of the E1 to E5 samples were about 228.1 Pa·s (Figure 13a). According to the testing results from series A to E, the influence of the base composition on the rotational viscosity was more significant than that of the solid particles. An increase in the particle size of the modifying particles increased the lowest adhesion coefficient from 0.108 to 0.131 (Figure 13b) and increased the slope of the friction characteristic from $0.012\%^{-1}$ to $0.041\%^{-1}$ (Figure 13c). The most significant increase in the adhesion coefficient occurred when the particle size exceeded 1 μm; however, this increase reached saturation after the particle size exceeded 8 μm.

With the mass content, the mass content ratio of lubrication particles to modifying particles, and the hardness of lubrication particles and modifying particles unchanged, the effect of the particle size of the modifying particles was equivalent to an increase in the volume proportion of kaolin particles, which is also equivalent to indirectly increasing the mass content of modifying particles and the hardness of kaolin particles. Therefore, the wheel-rail adhesion was increased by enhancing the shear strength of the FM third body layer. However, when the particle size of kaolin reaches a certain level, the particles are too easily crushed by wheel-rail forces. The experimental results indicate that the ideal maximum particle size of kaolin particles is 8 μm. To enhance the safety of the wheel-rail interface after applying FM, the kaolin particle

size was chosen as 8 μm to achieve a higher level of adhesion coefficient.

4. Discussion

4.1 Influencing factors for the friction control performance of FMs

Figure 14 shows the variation of the adhesion coefficient and images of the wheel-rail surfaces after applying an FM sample. It can be observed that the wheel-rail contact experiences different contact states under the FM condition. Initially, the application of an FM sample leads to the wheel-rail contact transforming from a dry state into a mixed lubrication state. Then, with the removal and drying of the FM third-body layer in the subsequent running cycles, the lubrication is rapidly starved, and the wheel-rail contact state turns into a boundary state. The residual FM third-body material adheres to the wheel and rail surfaces, maintaining some lubrication effect until it is completely exhausted. Potential influencing mechanisms regarding the friction control performance of FMs can be proposed as follows:

(1) The lowest adhesion coefficient – As only a small amount of the FM sample was used in the first type of test, the lowest adhesion coefficient occurred in a very short duration at the moment of applying the FM sample. The contact interface between the wheel-rail rollers was in a mixed lubrication state. The fluid viscosity is an important influencing factor for the adhesion coefficient based on Stribeck lubrication theories. For common lubricants (e.g., water, oil, etc.), their shear strength has a small effect on the adhesion coefficient as those values are almost negligible compared to the shearing force. For FMs that contain a lot of solid particles, the shear strength of the fluid is improved by the internal friction of these particles, which can help increase the lowest adhesion coefficient.

(2) Retentivity – The duration of the influence of the FM was evaluated by the adhesion

recovery process, which can be further divided into a rapid recovery stage and a slow recovery stage. In the rapid recovery stage, the recovery of the adhesion coefficient primarily resulted from the mixed lubrication along with mechanical exhaustion (splash loss, flow loss, etc.) and the drying process of the FM samples. The drying rate was highly dependent on the volatility of the liquid (water and resin). A high mass content of resin accelerated the drying rate of the FM sample due to its lower film-forming temperature. Although the retentivity of the FM could be prolonged by increasing the mass content of resin, excess resin increased the likelihood of the FM sample being squeezed out of the wheel-rail contact zone and drying out, as observed in previous studies [23]. In the slow recovery stage, the FM was in a dried state, and non-volatile residues formed in the third-body layer on the wheel and rail surfaces. Under these conditions, the adhesion recovery process primarily resulted from the removal of FM third-body layers by wheel-rail forces. Thus, the retentivity of the residual FM third-body layers was limited by its shear strength in the slow recovery stage.

(3) Creep curve - The creep curve was measured under the condition that an FM third-body film covered the wheel and rail surfaces. Based on the third-body layer model [33], the adhesion coefficient is determined by the shear strength of the third-body layer. This value can be much higher than that of fluid lubrication films and keeps being improved along with the wheel-rail force (positive friction). Therefore, the shear strength of the third-body layer of the dried FM appears to be the major factor influencing the friction characteristic.

Additionally, the test and analysis results suggest that the friction control performance of FM is influenced by a combined effect of the application amount, the third-body contamination layer, and solid particles in FM. In the FM application process in the field, excessive application

of FM may lead to wheel-rail damage and accelerate crack propagation, while excess FM can also cause environmental pollution. Conversely, insufficient application of FM can reduce its friction control performance. Based on the test results, it is inferred that FM application amount and solid particles may be two interdependent parameters. For example, an FM with a higher concentration of lubricating particles may achieve an ideal adhesion coefficient with a reduced application amount.

Besides, its friction control performance will be affected by contamination layers such as water, oil, and leaves. On the one hand, the presence of these contamination layers will further reduce the adhesion coefficient of the wheel-rail interface under FM conditions. For example, Skurka et al. [34] found that water can reduce the adhesion coefficient to 0.35 using a under FM conditions. Therefore, it is necessary to be cautious in applying FM in rainy or snowy environments to avoid affecting the safety of the train. On the other hand, by changing the solid particle parameters in FM (such as hardness and particle size), it is possible to make FM exhibit adhesion enhancer similar to those of traction enhancer products [35, 36]. The high-hardness solid particles contained in FM can produce a ploughing effect on the wheel-rail surface, thereby accelerating the removal rate of the contamination layer and the recovery rate of the adhesion coefficient [35].

4.2 The roles of solid particles in the water-based FM

The above analysis and testing results indicate that the shear strength of FM third body material is a key parameter affecting its friction control performance. The solid particles in FM can significantly alter the shear strength of the FM third body layer. A schematic of the internal structure of typical FM samples is proposed in Figure 15. Regarding the properties of FM

samples, the short retentivity and the potential risk of low adhesion are disadvantages during the application process. For FM samples without modifying particles, the characteristics of the fluid carriers determine their shear strength and drying rate. Water (A1) or CMC solution (A3) relatively prolongs the drying time, but their low viscosity and poor film-forming properties do not meet the application requirements for FM products. In contrast, resin (A2) increases the drying rate and film-forming properties of the samples, thereby improving the retentivity of the FM samples, but it also raises the risk of low adhesion. Therefore, it is necessary to design the content of resin and water appropriately to provide suitable drying time and adequate retentivity for the FM sample. Considering that resin primarily adheres solid particles to the surface of wheel-rail rollers after the FM third body layer is completely dried, the ratio of resin to solid particles is set to 1:1, with the remaining suspension effect provided by a 3.6% mass fraction of CMC aqueous solution.

The influence mechanism of solid particles on the friction control performance of FM samples can be explained using Coulomb's law of shear (Equation 3):

$$\tau_n = c + \sigma_n \times tan\,\varphi \tag{3}$$

, where τ_n (kPa) is the shear strength; c (kPa) is the material inside cohesion; σ_n (kPa) is the normal load; φ (°) is the internal friction angle. According to Equation 3, the shear strength τ_n of FM samples depends on the cohesive force of the material, normal load, and the internal friction angle. The material internal cohesion c of FM samples includes not only the basic cohesive force provided by the suspension system but also the van der Waals forces between all material molecules. The normal force σ_n comes from the normal load applied between the wheel-rail interface. The internal friction angle φ depends on the mass fraction, ratio, hardness,

and particle size of solid particles.

By varying the mass fraction, ratio, hardness, and particle size of solid particles, it is possible to alter the material internal cohesion c and internal friction angle φ of the FM samples. For FM samples in series B, both talc particles and graphite particles have relatively low Mohs hardness. An increase in the mass fraction of solid particles not only increases the viscosity but also reduces the internal friction angle φ. Consequently, the adhesion coefficient level decreased as the shear strength decreased (Figure 10d). In the case of the C series FM samples, talc particles have a higher Mohs hardness compared to graphite particles and possess an irregular shape (Figure 1d). Figure 16 shows the SEM images of typical FM samples in series A and C. From Figure 16, it can be seen that the surface roughness of FM samples increased as the mass content of talc particles increased, which may indicate a higher internal friction angle φ. Therefore, increasing the mass fraction of talc particles (A7 and C5) can enhance the internal friction angle φ and shear strength τ_n of an FM. This leads to an increased lowest adhesion coefficient and decreased retentivity.

However, the improvement of the adhesion coefficient through the application of FM samples is limited due to the relatively low Mohs hardness of talc particles. Therefore, talc particles were replaced with harder modifying particles. The experimental results from the FM samples in series D demonstrate that this approach is more effective for adjusting the friction control performance of FM samples. By increasing the particle size of modifying particles, the van der Waals forces between the modifying particles can be increased, enhancing the material internal cohesion c and shear strength τ_n. However, once the particle size exceeds a certain value, its impact on shear strength τ_n reaches a saturation point, which may be attributed to the

breakage of larger modifying particles under the action of wheel-rail forces.

Through the above analysis and experiments, E4 demonstrates excellent friction control performance. This sample was produced by adding 12.17% resin, 3.04% graphite particles, and 9.13% kaolin particles with a diameter of 8.5 μm into a 3.6% CMC solution. It can adjust the lowest adhesion coefficient to 0.129 and generate an obvious positive positive friction. Its retentivity at the wheel-rail interface is approximately 457 cycles. On railway lines, a wheel-rail adhesion coefficient above 0.15 is considered adequate adhesion, while a range of 0.1~0.15 is classified as moderate adhesion. A wheel-rail adhesion coefficient below 0.10 is regarded as low adhesion, and below 0.05 as severely low adhesion [27, 37]. Therefore, the adhesion coefficient of 0.129 generated by applying E4 sample falls within the moderate adhesion range, which can meet the normal traction and braking requirements. Furthermore, a comparison of the mass fraction, ratio, hardness, and particle size of solid particles shows that increasing the hardness of the modifying particles has the most significant impact on the adhesion behavior of the wheel-rail interface.

5. Conclusions

In this study, five series of FM samples were prepared by varying fluid carriers, mass fractions, ratios, hardness, and particle sizes of solid particles. Their friction control performances were tested and compared using a twin-disc testing apparatus. The main conclusions of this paper are as follows:

(1) The characteristics of fluid carriers significantly influence their shear strength and drying rate. Water or CMC solutions prolong the drying time of FM samples. In contrast, resin enhances both the drying rate and film-forming properties. Therefore, it is essential to carefully

balance the mass content of resin and water to achieve an optimal drying rate and sufficient basic retentivity for FM samples.

(2) There are strong correlations among the lowest adhesion coefficient, retentivity, adhesion coefficient recovery speed, and creep curve. Pearson correlation analysis revealed that both the lowest adhesion coefficient and the York linear regression slope are effective indicators of the adhesion behavior of the wheel-rail interface after the application of FM samples.

(3) The impact of solid particles on the friction control performance of FM samples can be explained using Coulomb-Mohr shearing law. By varying the mass fraction, ratio, hardness, and particle size of the solid particles, the internal cohesion c and internal friction angle φ of FM samples can be effectively altered.

(4) By varying the mass content, the mass content ratio of lubrication particles to modifying particles, hardness, and particle size of modifying particles, the internal cohesion c and internal friction angle φ of FM samples can be effectively altered, thereby optimizing friction control performance of FM samples. The hardness of the modifying particles has the most significant impact on the adhesion behavior of the wheel-rail interface.

(5) The FM sample, produced by mixing 12.17 % resin, 3.04 % graphite particles, and 9.13 % kaolin particles with a diameter of 8.5 μm into a 3.6 % CMC aqueous solution, can adjust the lowest adhesion coefficient to 0.129 and generate relatively obvious positive creep curve, exhibits desired friction control performance.

Acknowledgment

The work was supported by National Natural Science Foundation of China (Nos. 52272443, 52320105007, 52027807) and Fundamental Research Funds for the Central

Universities (No. 2682024CG007).

Declaration of interest statement

The authors declare that they have no known competing financial interests or personal relationships that could have appeared to influence the work reported in this paper.

References

[1] Hu Y, Zhou L, Ding H, et al. Microstructure evolution of railway pearlitic wheel steels under rolling-sliding contact loading. Tribology International. 2020; 154: 106685.

[2] Zhang S, Spiryagin M, Ding H, et al. Rail rolling contact fatigue formation and evolution with surface defects. International Journal of Fatigue. 2022; 158: 106762.

[3] Lu X, Makowsky TW, Eadie DT, et al. Friction management on a Chinese heavy haul coal line. Proceedings of the institution of mechanical engineers part F: Journal of rail and rapid transit. 2012; 226: 630-640.

[4] Lundberg J, Rantatalo M, Wanhainen C, et al. Measurements of friction coefficients between rails lubricated with a friction modifier and the wheels of an IORE locomotive during real working conditions. Wear. 2015; 324-325: 109-117.

[5] Reiff R, Cotter J, Elvidge D. Prototype Demonstration Freight Car-based Top of Rail Friction Modifier ApplicationSystem. In: Proceedings of 8th International Heavy Haul Railway Conference. Rio de Janeiro, Brazil, 2005.

[6] Stock R, Stanlake L, Hardwick C, et al. Material concepts for top of rail friction management - Classification, characterisation and application. Wear. 2016; 366-367: 225-232.

[7] Hardwick C, Lewis R, Stock R. The effects of friction management materials on rail with

pre existing rcf surface damage. Wear. 2017; 384-385: 50-60.

[8] Tian Y, Daniel WJT, Meehan PA. Real-Time rail-wheel wear damage control. International Journal of Rail Transportation. 2016; 4(2): 113-129.

[9] Meehan PA, Liu X. Wheel squeal noise control under water-based friction modifiers based on instantaneous rolling contact mechanics. Wear. 2019; 440: 203052.

[10] Matsumoto A, Sato Y, Ohno H, et al. Improvement of bogie curving performance by using friction modifier to rail/wheel interface Verification by full-scale rolling stand test. Wear. 2005; 258: 1201-1208.

[11] VanderMarel J, Eadie DT, Oldknow KD, et al. A predictive model of energy savings from top of rail friction control. Wear. 2014; 314: 155-161.

[12] Zirek A, Onat A. A novel anti-slip control approach for railway vehicles with traction based on adhesion estimation with swarm intelligence. Railway Engineering Science. 2020; 28(4): 346-364.

[13] Egana JI, Vinolas J, Gil-Negrete N. Effect of liquid high positive friction (HPF) modifier on wheel-rail contact and rail corrugation. Tribol International. 2005; 38: 769-774.

[14] Pan Y, Radmehr A, Ahmadian M. Experimental evaluation of amount and repeated applications of top of rail friction modifiers on wear and adhesion. International Journal of Rail Transportation. 2022; 11(6): 855-871.

[14] Wu B, Shi L, Ding H, et al. Influence of different solid particles in friction modifier on wheel-rail adhesion and damage behaviours. Wear. 2023; 522: 204833.

[15] Sroba P, Oldknow K, Dashko R, et al. Canadian Pacific Railway 100% effective friction management strategy. In: Proceedings of the 8th International Heavy Haul Railway

Conference, Rio de Janeiro, Brazil, 2005.

[16] Galas R, Kvarda D, Omasta M, et al. The role of constituents contained in water-based friction modifiers for top-of-rail application. Tribology International. 2018; 117: 87-97.

[17] Kvarda D, Skurka S, Galas R, et al. The effect of top of rail lubricant composition on adhesion and rheological behaviour. Engineering Science and Technology, an International Journal. 2022; 35: 101100.

[18] Zakharov SM, Goryacheva IG, Krasnov AP, et al. Tribological studies for developing friction modifiers in the wheel-rail system. Journal of Friction and Wear. 2015; 36: 468-475.

[19] Matsumoto A, Sato Y, Ono H, et al. Creep force characteristics between rail and wheel on scaled model. Wear. 2002; 253: 199-203.

[20] Lu X, Cotter J, Eadie DT. Laboratory study of the tribological properties of friction modifier thin films for friction control at the wheel/rail interface. Wear. 2005; 259: 1262-1269.

[21] Wang J. Study on the dispersity and stability of graphite aqueos (in Chinese). Doctoral thesis: Suzhou University, 2006.

[22] Anushree C, Abdul Rahim F, Vanithakumari SC, et al. Electrospun superparamagnetic fibrous composite nanofiber films for enhanced oil spill recovery: Effect of capping and magnetic nanoparticle loading on oil sorption efficiency. Composites Part A: Applied Science and Manufacturing. 2023; 171: 107591.

[23] Wu B, Shi L, Li J, et al. Tribological and rheological performance of friction modifiers with different viscosities. Wear. 2023: 205229.

[24] Ding H, Jiang S. Comparative study on tribological properties of isostatic graphiteand carbon graphite under dry sliding and water-lubricated conditions. Journal of Southeast University (English Edition). 2020; 36: 273-277.

[25] Xavier YL, Rezende AB, Fonseca ST, et al. Study of the initial cycles number Influence on the retentivity of a commercial friction modifier using the Twin-disk Test. Tribology Transactions. 2024: 67(2): 212-221.

[26] Gutsulyak DV, Stanlake LJE, Qi H: Twin disc evaluation of third body materials in the wheel/rail interface. Tribology-Materials, Surfaces and Interfaces. 2021; 2(15): 115-126.

[27] Shi L. Study on the adhesion enhancement and damage behaviours of wheel/ rail in the application of hard particles (in Chinese). Doctoral thesis: Southwest Jiaotong University, 2020.

[28] Beagley T, Pritchard C. Wheel/rail adhesion—the overriding influence of water. Wear. 1975; 35: 299-313.

[29] Verma SP, Diaz-Gonzalez L, Sanchez-Upton P, et al. OYNYL: a new computer program for ordinary, York, and New York least-squares linear regressions. WSEAS Transactions on Environment and Development. 2006; 2: 997-1002.

[30] Benesty J, Chen J, Huang Y, et al. Pearson Correlation Coefficient. In: Noise Reduction in Speech Processing. Springer Topics in Signal Processing, vol 2. Springer, Berlin, Heidelberg.

[31] Li Q, Wu B, Ding H, et al. Numerical prediction on the effect of friction modifiers on adhesion behaviours in the wheel-rail starved EHL contact. Tribology International. 2022; 170: 107519.

[32] Li Q, Zhang S, Wu B, et al. Analysis on the effect of starved elastohydrodynamic lubrication on the adhesion behavior and fatigue index of wheel-rail contact. Wear. 2022; 510-511: 204506.

[33] Chen H, Ban T, Ishida M, et al. Adhesion between rail/wheel under water lubricated contact. Wear. 2002; 253: 75-81.

[34] Skurka S, Galas R, Omasta M, et al. The performance of top-of-rail products under water contamination. Tribology International. 2023; 188: 108872.

[35] Li Z, Arias-Cuevas O, Lewis R, et al. Rolling-sliding laboratory tests of friction modifiers in leaf contaminated wheel-rail contacts. Tribology Letter. 2009; 33: 97-109.

[36] Lewis SR, Lewis R, Cotter J, et al. A new method for the assessment of traction enhancers and the generation of organic layers in a twin-disc machine. Wear. 2016; 366-367: 258-267.

[37] Vasic G, Franklin FJ, Kapoor A, et al. Laboratory simulation of low-adhesion leaf film on rail steel. International Journal of Surface Science and Engineering. 2008; 2(1-2): 84-97.

Table 1 Detailed information about five series of FM samples

Series	No.	Water	CMC	Resin	Lubrication particles	The type of lubrication particles	Modifying particles	The type of modifying particles
A	1	100	0	0	0		0	
	2	0	0	100				
	3	96.5	3.5	0				
	4	50	0	50				
	5	78.5	3.5	20				
	6	76.31	2.77	10.46	10.46		0	
	7	76.31	2.77	10.46	0		10.46	
B	1	77.48	2.81	10.46	4.625	Graphite	4.625	Talc
	2	76.31	2.77		5.23		5.23	
	3	74.78	2.71		6.025		6.025	
	4	72.71	2.64		7.095		7.095	
	5	69.77	2.53		8.62		8.62	
C	1	76.31	2.77	10.46	5.23		5.23	
	2				3.49		6.97	
	3				2.615		7.845	
	4				2.095		8.368	
	5				1.74		8.72	
D	1	76.31	2.77	10.46	3.04		9.13	Talc
	2							Zinc oxide
	3							Kaolin
	4							Silicon dioxide
	5							Aluminum oxide
E	1	76.31	2.77	10.46	3.04		9.13	Koalin (0.8μm)
	2							Koalin (1μm)
	3							Koalin (2.6μm)
	4							Koalin (8.5μm)
	5							Koalin (12μm)

Table 2 Chemical compositions of wheel and rail rollers.

Component	Grade	wt% of chemical composition					Bulk hardness/$HV_{0.5}$
		C	Si	Mn	P	S	
Wheel	C-class	0.67-0.77	0.15-1.0	0.60-0.90	0.030	0.005-0.040	345±10
Rail	U75V	0.71-0.80	0.50-0.80	0.70-1.05	≤0.030	≤0.030	303±14

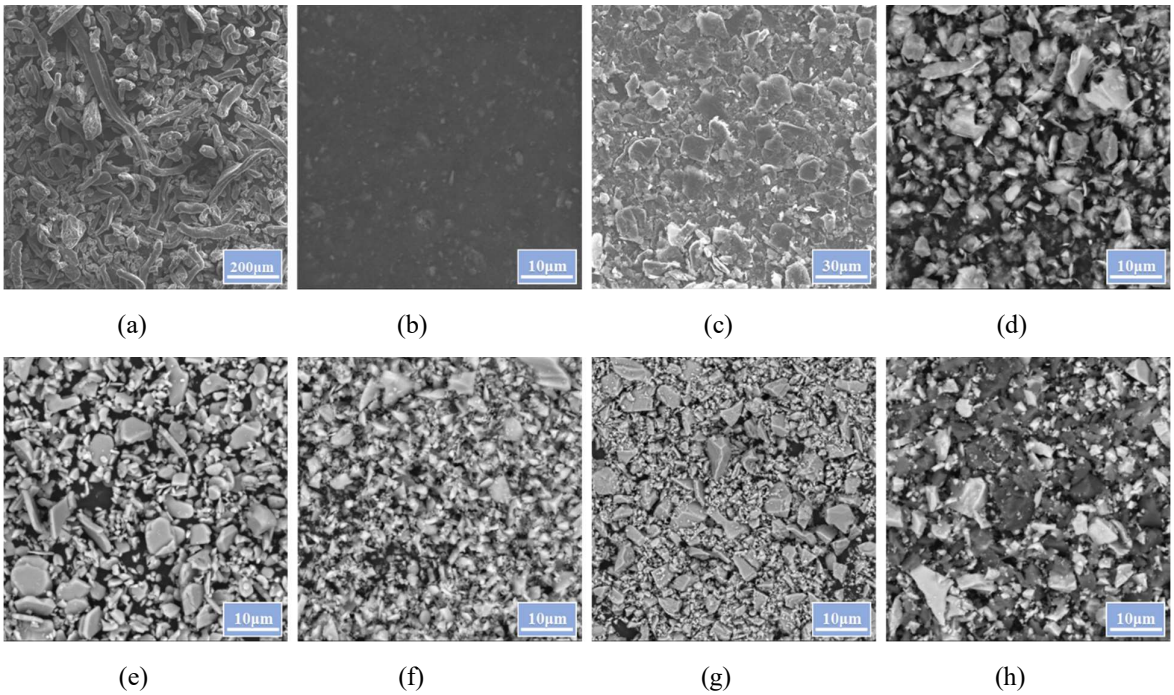

Fig.1 SEM images of constituents used for preparing FM samples: (a) carboxymethyl cellulose (CMC); (b) dried acrylic resin emulsion; (c) graphite particles; (d) talc particles; (e) aluminum oxide particles; (f) silicon dioxide particles; (g) kaolin particles; (h) zinc oxide particles

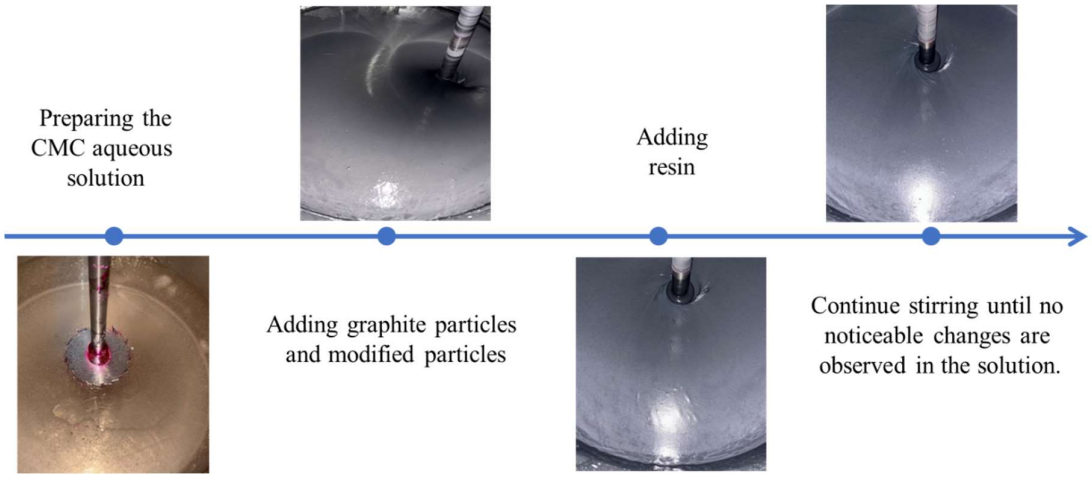

Fig.2 Schematic diagram of the preparation process of FM

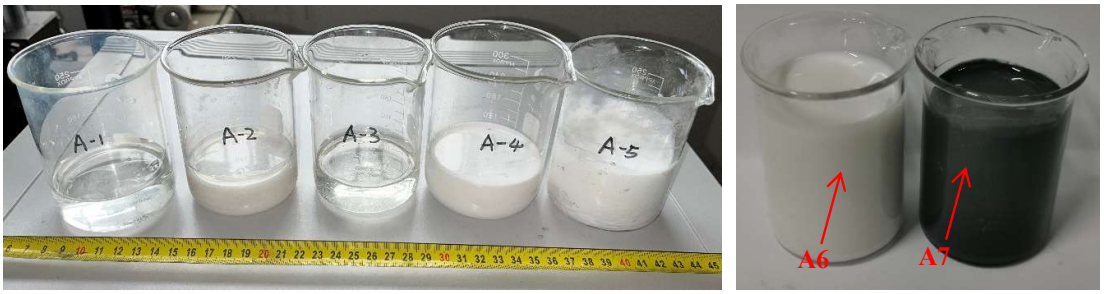

Fig.3 The appearance of series A FM samples (A6 and A7 had a different appearance due to the addition of graphite and talc respectively which are not in A1 to A5)

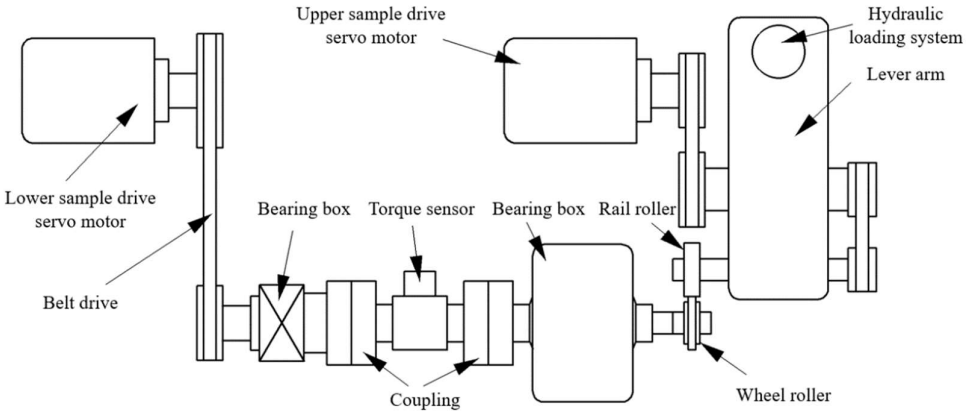

(a)

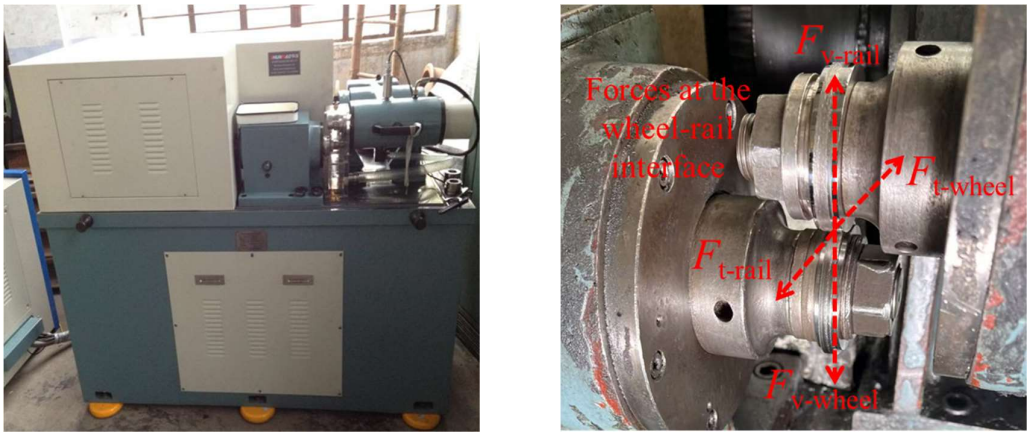

(b) (c)

Fig.4 Schematic of (a) the twin-disc testing apparatus and the images of (b) the twin-disc testing apparatus and (c) the twin-disc contact area

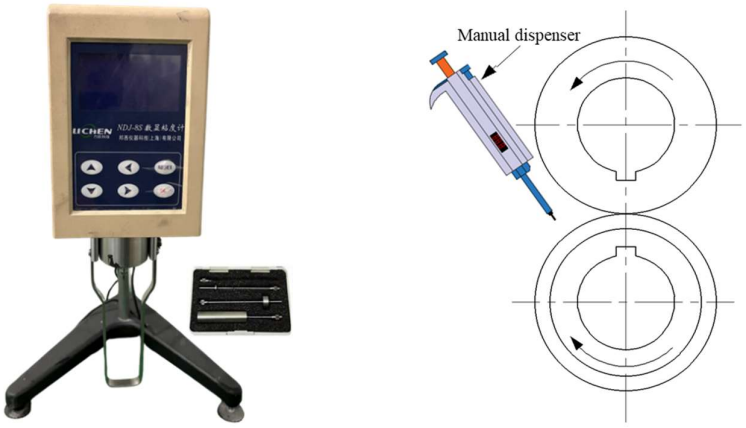

(a) (b)

Fig.5 Schematics of (a) the rotational viscometer and (b) the application method of FM samples

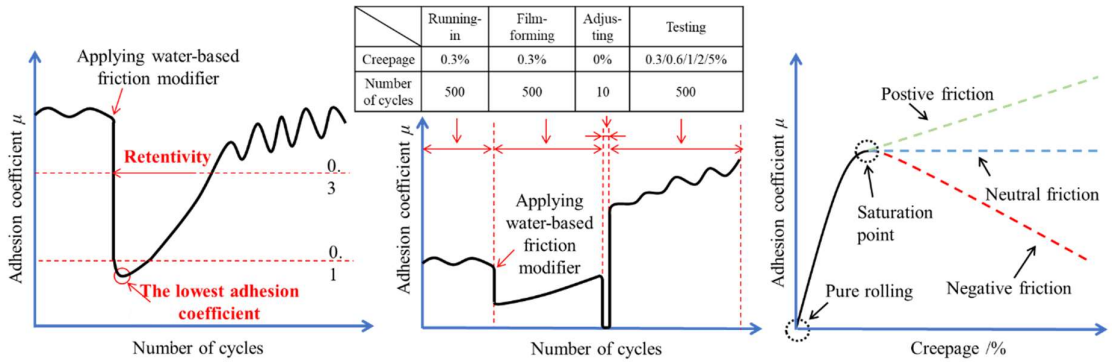

(a) (b) (c)

Fig.6 Adhesion curve Schematics of (a) the lowest adhesion coefficient and retentivity test, (b) the creep curve test, and (c) the creep curve type

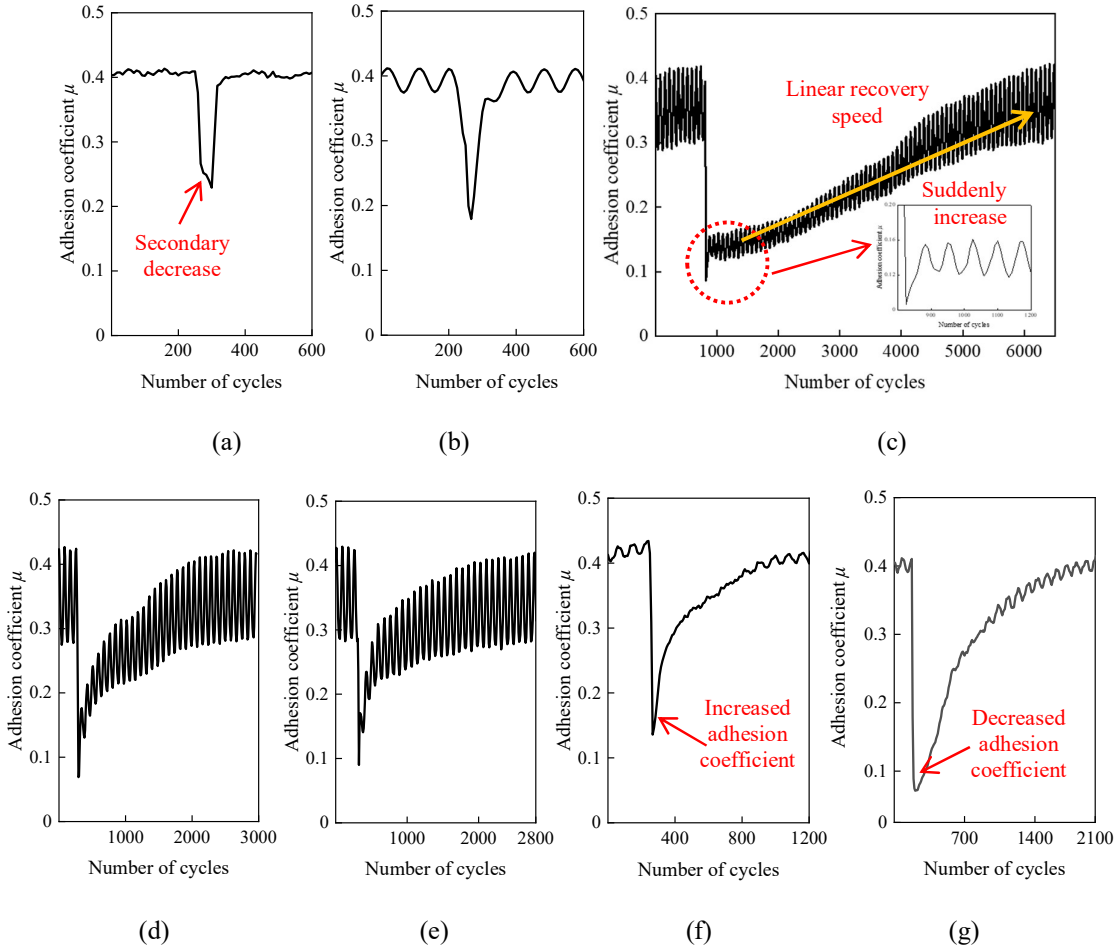

(a) (b) (c)

(d) (e) (f) (g)

Fig.7 Adhesion coefficient curves obtained in the first type of test: (a) A1; (b) A3; (c) A2; (d) A4; (e) A5; (f) A6; (g) A7

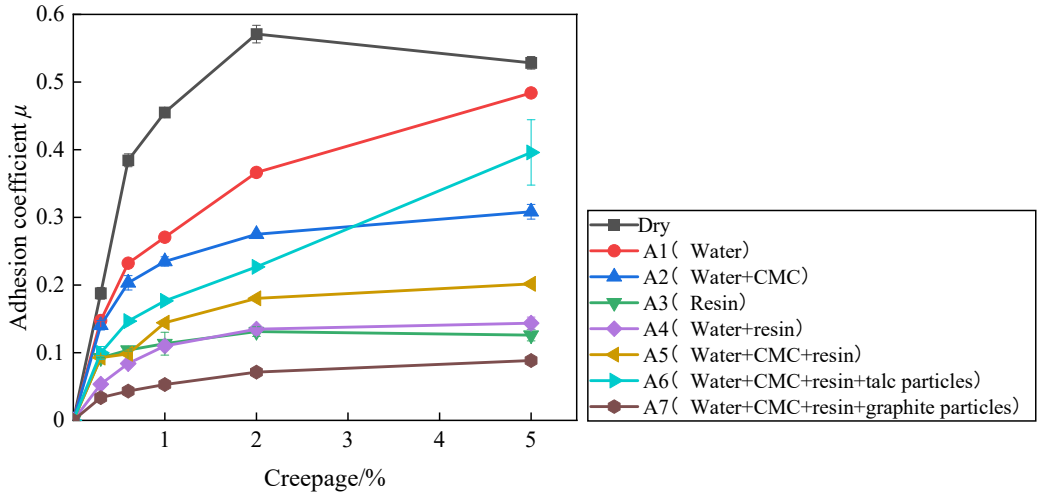

Fig.8 Creep curves obtained in the first type of test for series A of FM samples

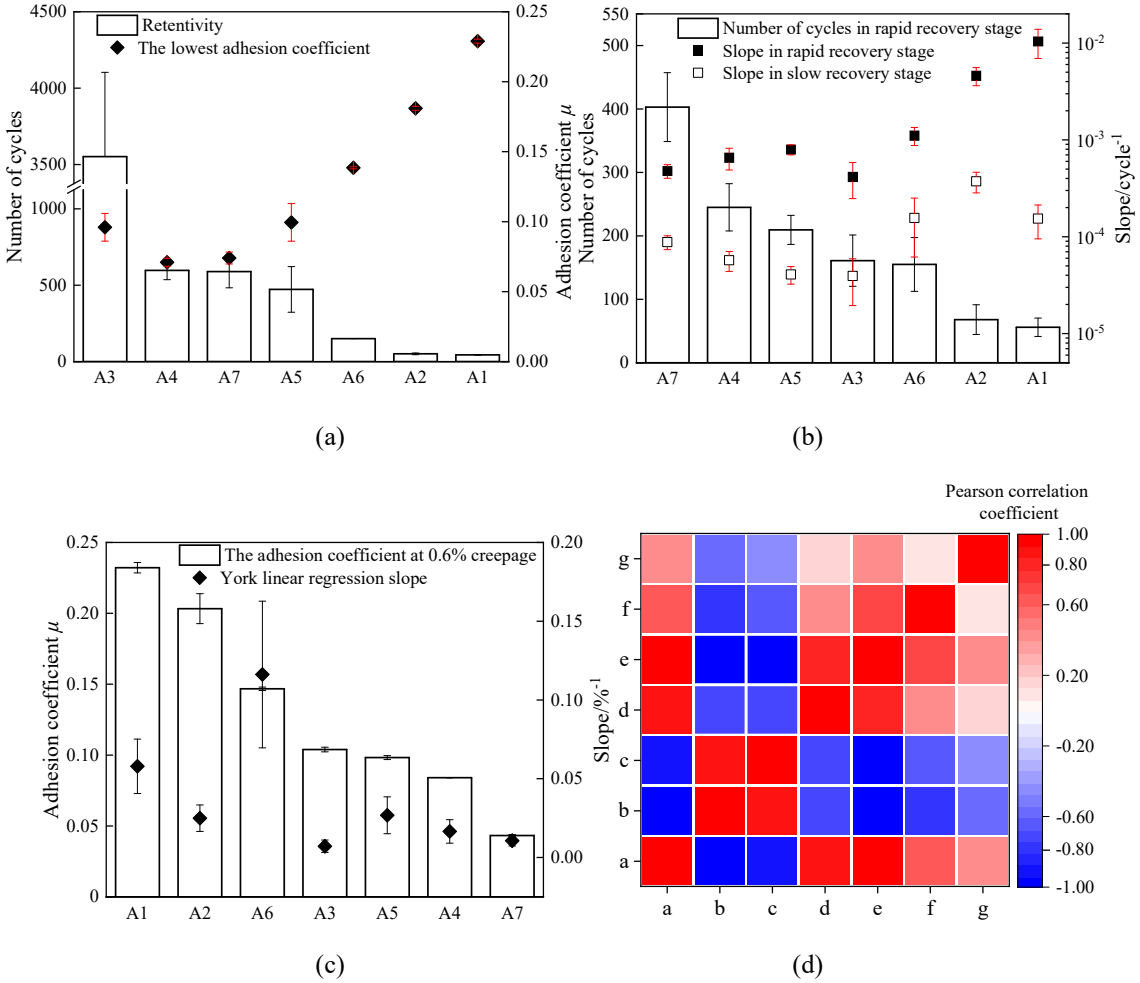

Fig.9 Statistical results of applying series A: (a) the lowest adhesion coefficient and retentivity; (b) adhesion recovery speed parameters; (c) friction characteristic parameters; (d) Pearson correlation coefficients between every parameter (Darker colors indicate a higher degree of correlation; red represents

positive correlation, while blue represents negative correlation).

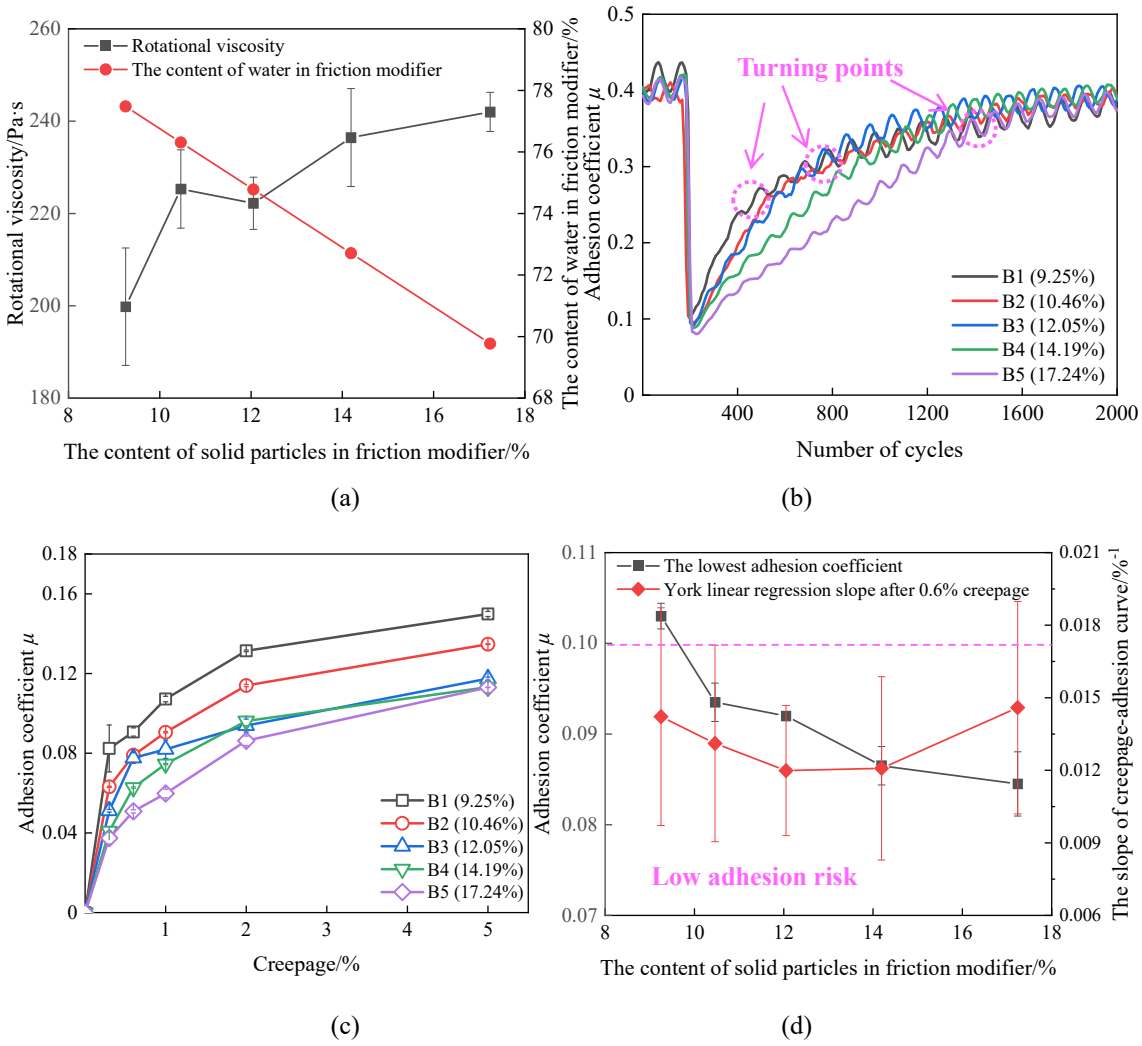

Fig.10 Series B of FM samples: (a) rotational viscosities; (b)adhesion coefficient curve; (c) creep curve; (d) the lowest adhesion coefficient and York linear regression slope

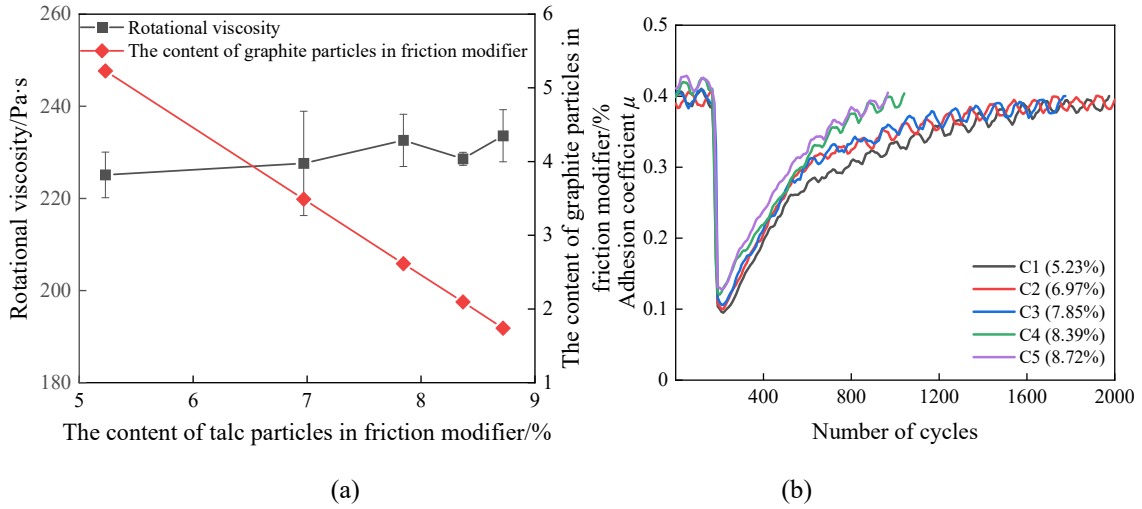

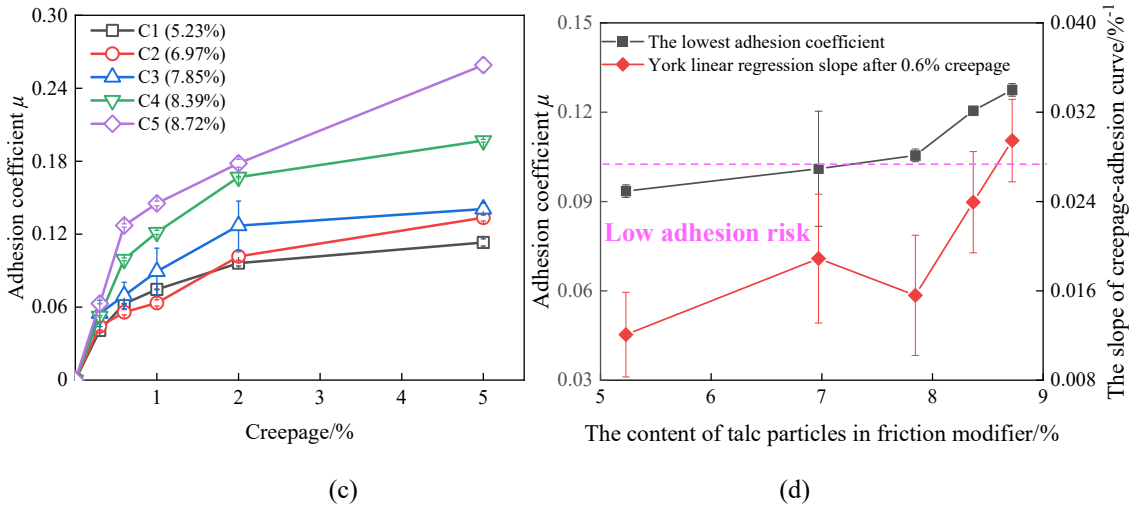

(c) (d)

Fig.11 Series C of FM samples: (a) rotational viscosities; (b)adhesion coefficient curve; (c) creep curve; (d) the lowest adhesion coefficient and York linear regression slope

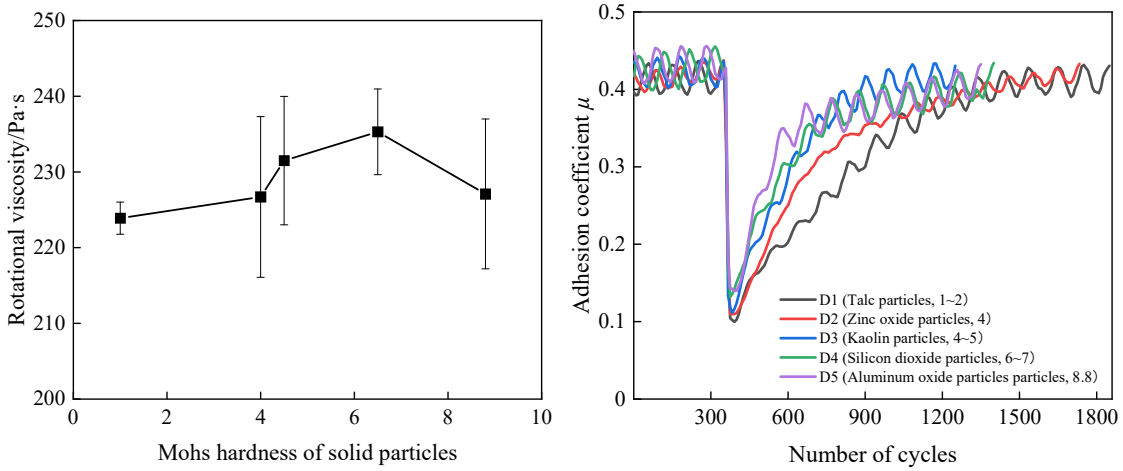

(a) (b)

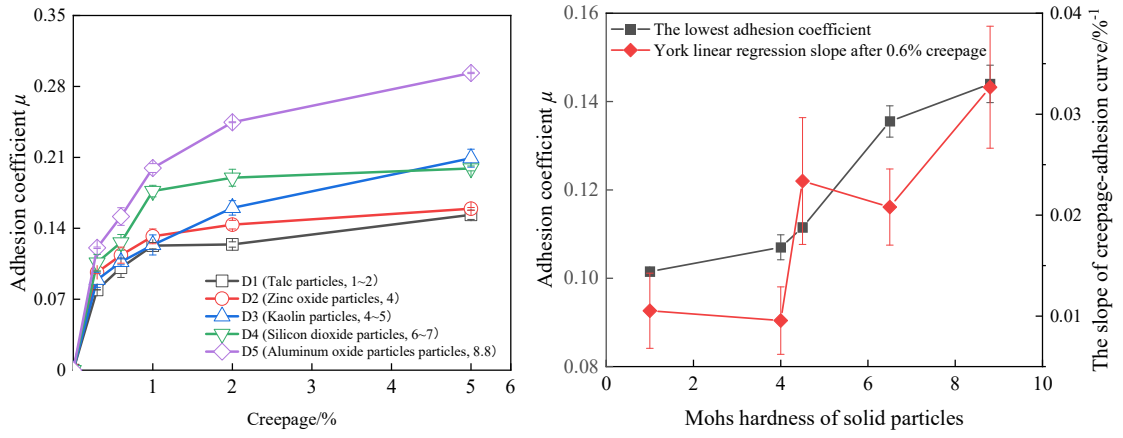

(a) (b)

Fig.12 Series D of FM samples: (a) rotational viscosities; (b)adhesion coefficient curve; (c) creep curve; (d)

the lowest adhesion coefficient and York linear regression slope

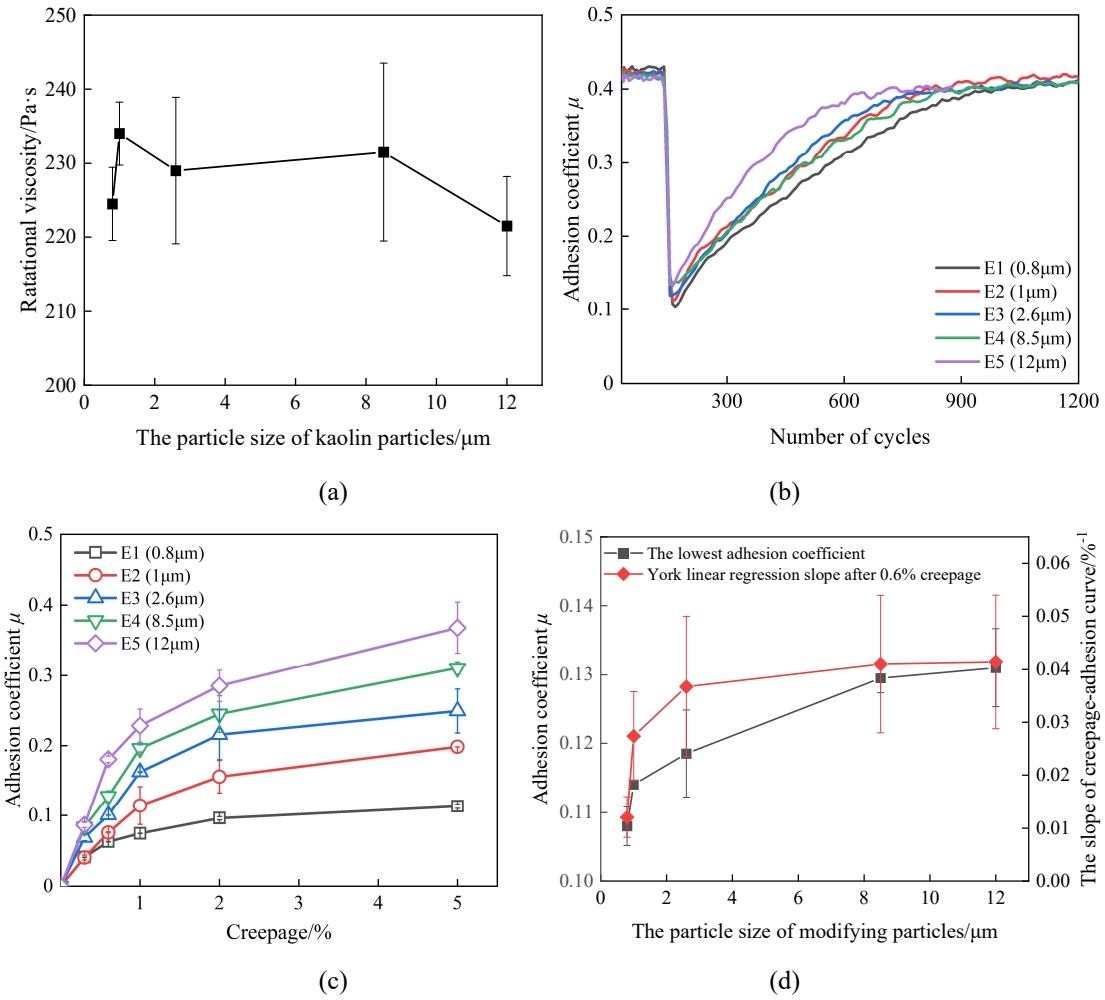

Fig.13 Series E of FM samples: (a) rotational viscosities; (b)adhesion coefficient curve; (c) creep curve; (d) the lowest adhesion coefficient and York linear regression slope

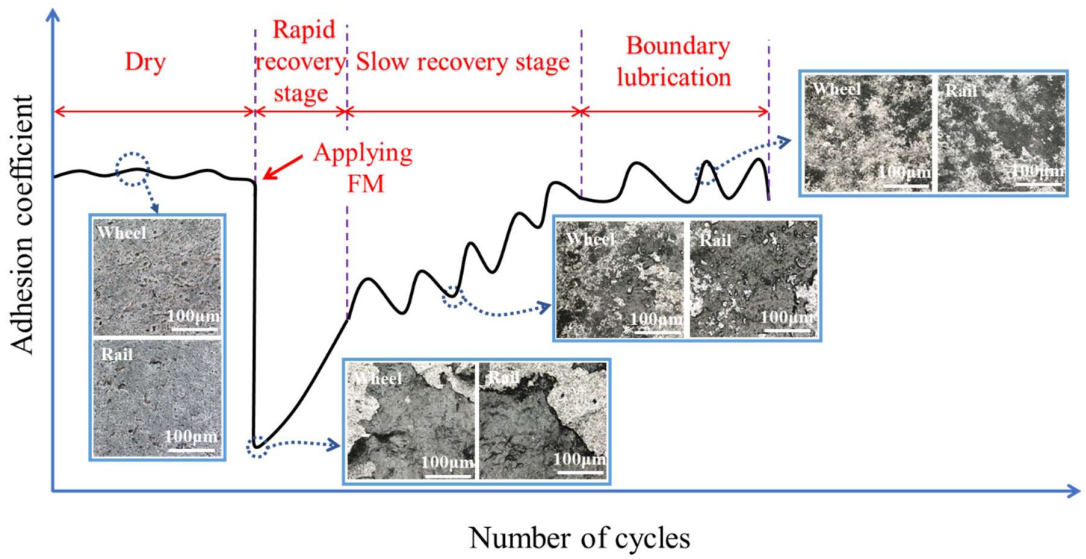

Fig.14 Schematic of adhesion coefficient recovery process after applying FM and the images of wheel-rail rollers surfaces.

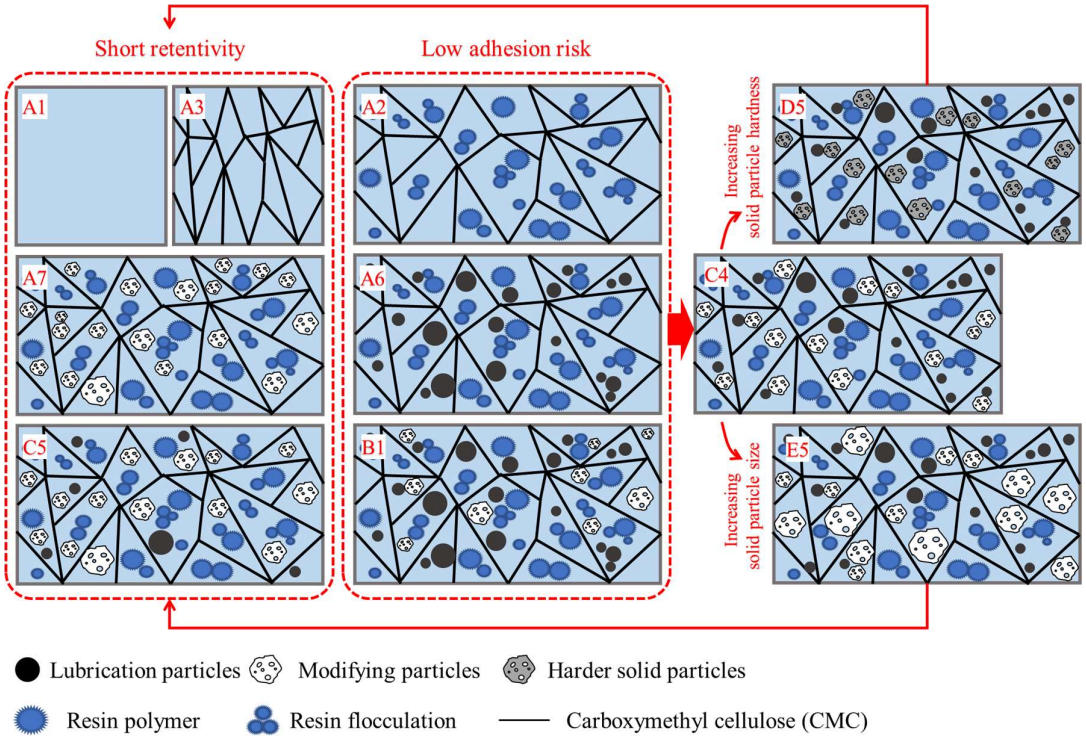

Fig.15 Schematic of the internal structure of typical FM samples

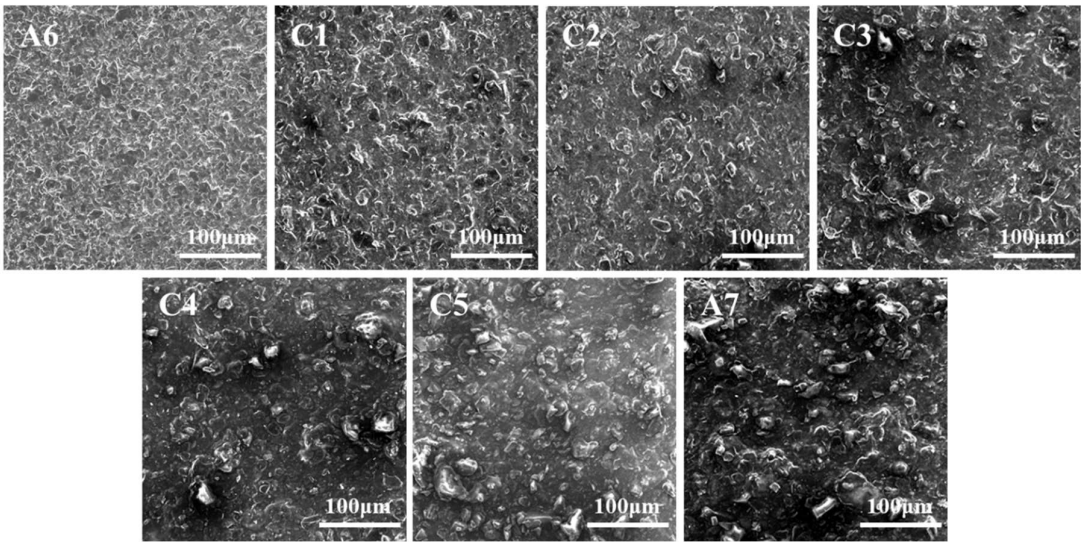

Fig.16 SEM images of typical FM samples in series A and C (the mass content of talc particles increased from A6, C1, C2, C3, C4, C5, A7)